Structural characterization of selective area growth GaN nanowires by non-destructive optical and electrical techniques

2015 J. Phys. D: Appl. Phys. 48 305301

(http://iopscience.iop.org/0022-3727/48/30/305301)

IOP Publishing Journal of Physics D: Applied Physics
J. Phys. D: Appl. Phys. **48** (2015) 305301 (6pp) doi:10.1088/0022-3727/48/30/305301

Structural characterization of selective area growth GaN nanowires by non-destructive optical and electrical techniques

Eleonora Secco[1], Albert Minj[1], Núria Garro[1], Andrés Cantarero[1], Jaime Colchero[2], Arne Urban[3], Carla Ivana Oppo[3], Joerg Malindretos[3] and Angela Rizzi[3]

[1] Institut de Ciència dels Materials, Universitat de València, 46980 Paterna (València), Spain
[2] Facultad de Química, Departamento de Física, Universidad de Murcia, 30100 Murcia, Spain
[3] IV. Physikalisches Institut, Georg-August-Universität Göttingen, 37077 Göttingen, Germany

E-mail: eleonora.secco@uv.es

Received 13 February 2015, revised 27 May 2015
Accepted for publication 5 June 2015
Published 2 July 2015

Abstract

The growth selectivity and structural quality of GaN nanowires obtained by plasma-assisted molecular beam epitaxy on pre-patterned GaN(0001) templates are investigated by means of non-destructive techniques. Optimum control over the nanowire arrangement and size requires a pitch between the mask apertures below twice the diffusion length of Ga atoms. Lower pitches, however, seem to slightly diminish the structural quality of the material, as revealed by the increase of the Raman peak linewidths. The photoluminescence spectra of the nanowires show a considerable presence of basal plane stacking faults, whose density increases for decreasing nanowire diameter. The capabilities of Kelvin probe force microscopy for imaging these kind of defects are also demonstrated.

Keywords: nanowires, Raman scattering, Kelvin probe, stacking faults

(Some figures may appear in colour only in the online journal)

1. Introduction

GaN nanowires (NWs) offer many potential advantages for optoelectronic and photonic devices based on the versatility of the columnar geometry and a higher crystal quality as compared to two-dimensional thin layers [1]. Residual strain and most extended defects are absent from self-organized GaN NWs grown by metal-organic chemical vapor deposition (MOCVD) and molecular beam epitaxy (MBE) on different substrates [1, 2]. As a result, the optical emission spectra of such nano-objects show bright and sharp excitonic peaks [3, 4]. Concerning nano-device processing, the main drawback of self-organized growth is, however, the inhomogenous distribution of height, size, position, and orientation of the NWs. Selective area growth (SAG) on a substrate covered by a patterned inert mask appears as a good alternative for the growth of regular arrays of vertically aligned NWs with precise control over their height and diameter [5–11]. This growth process differs significantly from self-organized growth. As described by Urban *et al* in the case of SAG by MBE under highly N-rich conditions [12], initially multiple GaN nuclei form inside each of the mask apertures, growing in size and coalescing to form a pedestal. Then, semipolar facets start growing at the pedestal edges from the outside of the pedestals inwards until a hexagonal pyramidal tip is completed. The growth proceeds along the axial (semipolar) and radial (nonpolar) directions. In order to suppress the GaN nucleation directly on the mask, SAG requires high growth temperatures and well-defined Ga/N ratios [6]. The first studies of the structural quality of the material resulting from such a growth process showed that they are affected by threading dislocations and basal plane stacking faults (BSF) [12]. The direct detection of such defects, which is commonly carried out by transmission electron microscopy, requires a sophisticated preparation, which usually implies the partial destruction of the sample. The use of non-destructive techniques for

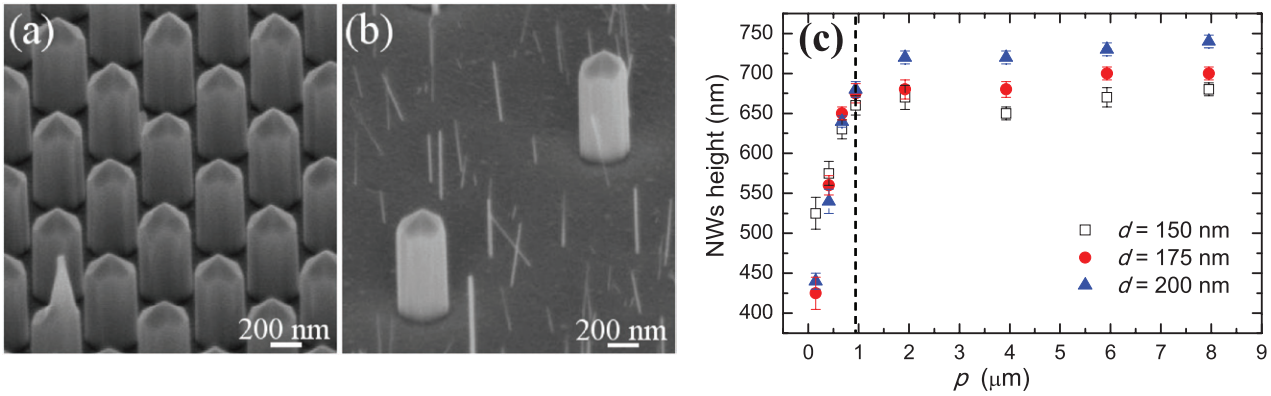

Figure 1. SEM micrographs (bird's eye view) of GaN NWs of hexagonal cross-section with pyramidal tips defined by $(1\bar{1}02)$ facets (r-plane). The two images correspond to (a) $d = 370$ nm and $p = 0.4$ μm and (b) $d = 370$ nm and $p = 2.2$ μm. (c) Average NW height as a function of p. The error bars indicate the standard deviation. The dashed line shows approximately the transition from the competitive to the isolated regimes.

the characterization of semiconductor nanostructures could therefore be highly beneficial but is still quite unexplored.

In this article the structural properties of SAG GaN NWs and their dependence on the inert mask layout are investigated by means of Raman scattering and photoluminescence (PL). We also exploit the capabilities of Kelvin probe force microscopy (KPFM) for the simultaneous measurement of the surface potential and the topography of the NWs with spatial resolution down to nanoscale. All of the proposed techniques are contact-less and non-destructive, offering great versatility for studying both single and arrays of NWs.

2. Experimental

Homoepitaxial SAG of GaN NWs has been carried out by plasma-assisted MBE on a GaN(0 0 0 1)/sapphire MOCVD template (dislocation density of 4×10^8 cm^{-1}). Prior to epitaxy, a 10 nm thick Mo layer evaporated on the substrate surface was patterned by e-beam lithography. The resulting mask layout contained different periodic triangular arrays of apertures with diameter and pitch (defined as the distance between edges of neighbor apertures) nominally ranging from 30 to 500 nm and 0.25 to 8 μm, respectively. MBE growth was performed under nominal N-rich conditions (N/Ga ~9) for a total time of 3 h and with a substrate temperature of 780 °C. Raman scattering and PL spectra were obtained using an optical microscope coupled to a T64000 triple spectrometer from Jobin-Yvon® and a nitrogen-cooled charge-coupled device detector. Microscope objectives of 100 and 40 magnification provided laser spot diameters of 1 and 4 μm for visible and UV excitation, respectively. The spectral resolution of the whole system was 1 cm^{-1} at 500 nm. KPFM experiments were performed with a NanoTec atomic force microscope (AFM) equipped with a phase-locked loopboard (PLL, bandwidth 2 kHz), which maintained the cantilever (5 N m^{-1} force constant, resonance frequency 160 kHz) at resonance. Topography was acquired using the oscillation amplitude as a feedback parameter (AM-mode). In order to measure the contact potential difference (V_{CPD}) a fixed ac voltage (1.5 V and 7 kHz) is applied between the Pt-coated AFM tip and the sample surface which is held at the ground potential. A second feedback adjusts the dc bias to minimize the electrostatic tip-sample interaction using the resonance frequency as the signal source. Tip-sample distance is estimated to be between 5 and 15 nm, resulting in V_{CPD} imaging with high spatial resolution (~40 nm) [13, 14]. The experiments were carried out at low relative humidity in ambient conditions.

3. Results and discussion

The scanning electron microscopy (SEM) images in figures 1(a) and (b) show the achievement of selective growth of GaN NWs. The diameter (d) and pitch (p) of the NWs are measured from the SEM images. For all the investigated d and p, SAG nanostructures have pyramidal endings defined by semipolar facets. Occasionally, some of the NWs present additional structure growing from the NW apex (see bottom left-hand corner of figure 1(a)). Due to the influence of adatom diffusion on SAG [15], the mask pitch has a strong effect on the growth selectivity and two growth regimes have been identified depending on the ratio between p and Ga diffusion length (λ). For $p \leqslant 2\lambda$ the competitive regime is observed, where adjacent NWs compete for the Ga atoms diffusing on the mask surface. For $p > 2\lambda$ the isolated regime occurs and the growth of NWs is independent from one another. In the isolated regime, much thinner self-organized GaN NWs (diameter ~10–20 nm) also grow on the Mo mask with a density of ~30 NWs μm^{-2}, see figure 1(b). The diameter of the SAG NWs exceeds the aperture diameter in both regimes, revealing that radial growth is low but never completely suppressed. On the other hand, the NW height, which is an indicator of the axial growth rate, increases with p from 425 nm to the saturated value of 750 nm for $p > 1$ μm, as shown in figure 1(c). This behavior in the NW height clearly points out the transition between the competitive and isolated regimes. The effective Ga diffusion length on the Mo mask can be estimated from the intersection of these regimes ($\lambda = 435 \pm 30$ nm).

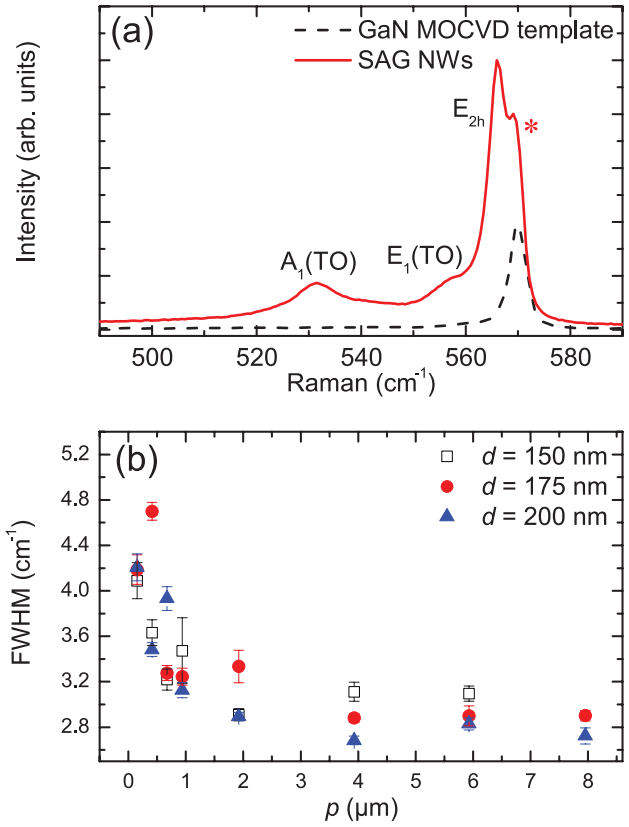

Figure 2. (a) Raman scattering spectra of GaN NWs ($d = 150$ nm, $p = 0.15$ μm) measured with 488 nm laser line excitation at room temperature. The peak marked with an asterisk corresponds to the GaN template. (b) Trend of the FWHM of the E_{2h} mode as a function of p for arrays of different d.

A first test of the quality of the GaN material has been carried out by Raman scattering spectroscopy. Figure 2(a) displays a representative Raman spectrum of SAG NWs. The most intense peak in all the spectra is that associated to the E_{2h} phonon of wurtzite GaN. Another distinctive feature of the Raman spectrum is the appearance of two additional peaks at ~533 cm^{-1} and ~557 cm^{-1}, matching the frequencies of the A_1(TO) and E_1(TO) modes of the hexagonal phase, respectively. Light scattering by TO modes is interpreted as an effect of the refraction of the incident laser beam at the pyramidal facets of the NW tip which results in an oblique internal excitation geometry. Moreover, the high refractive index of GaN (2.44) can cause multiple internal reflections of the excitation light that will also change the angle of the excitation and scattered light. It should be pointed out that the peak at ~557 cm^{-1} could also correspond to the TO mode of cubic GaN but the oblique penetration of light into the NWs makes it difficult to track the Raman selection rules and hampers the discrimination of the zinc-blende phase.

A closer analysis of the E_{2h} phonon of the GaN NWs can provide information about residual strain fields and the crystal quality of the material [16]. The E_{2h} peak is centered at a frequency of ~566.5 cm^{-1} for all p and d, which is in good agreement with the value of strain-free bulk samples [17], indicating that SAG NWs grow free of internal strain. The partial opacity of the Mo mask (92% and 72% measured for UV and visible light, respectively) allowed a weak peak attributed to the E_{2h} mode of the GaN MOCVD template to appear in the Raman spectrum. This peak is centered at 570 cm^{-1}, revealing that the slight residual compression of the substrate ($\sim -0.2\%$ assuming biaxial strain) is not transmitted into the NW material. The full width at half maximum (FWHM) of the E_{2h} peak and its dependence with p and d is a good indicator of the crystal quality of the material as a function of the mask layout and is shown in figure 2(b). While no significant variation is observed as a function of d (results not shown), the evolution of the FWHM as a function of p shows an abrupt change for $p \sim 1$ μm when the growth changes from isolated to competitive regimes. For $p > 1$ μm, FWHMs are similar to those measured for self-organized NWs, revealing a high crystalline quality of the SAG NWs. The much smaller total volume of the self-organized NWs (between 7.5 and 13 times lower than the volume of one SAG NW) makes their contribution to the Raman signal negligible. On the other hand, a pronounced increase in the FWHM with decreasing p is observed for $p < 1$ μm. The measured phonon broadenings, which remain below the 9 cm^{-1} FWHM of the E_{2h} mode of the GaN MOCVD template, correlate with the evolution of the NW height reported in figure 1(c) and suggest a decreasing density of structural defects with increasing NW height. This is in good agreement with TEM images of Urban *et al* showing how the threading dislocations originated in the base region bend and terminate at the nonpolar lateral surfaces of the NWs [12]. Consequently, longer NWs should present a lower density of dislocations. The origin of these defects is attributed to the coalescence of multiple GaN nuclei in the initial stages of the growth. Therefore we cannot exclude the effects of inhomogeneous microstrain arising from coalescence [18]. The latter contribution, however, cannot account for more than 2 cm^{-1}, assuming microstrain fields $\sim \pm 0.04\%$ as deduced from the PL linewidth (see below).

PL spectroscopy is another sensitive probe for the presence of structural defects. A representative low temperature PL spectrum of an array of SAG GaN NWs is shown in figure 3(a). Two distinctive UV peaks are observed at 3.471 eV and 3.42 eV, while no yellow luminescence, associated to nitrogen vacancies and other defects, has been observed. The most intense peak is attributed to the recombination of donor-bound excitons (D^0X_A). This peak presents a slight asymmetry at both the high and low energy sides which are compatible with traces of free A-exciton emission and two electron satellite processes [4], respectively. The D^0X_A energy position confirms that the SAG nanostructures are free from macroscopic strain. The large FWHM measured for this transition (~5.5 meV) exceeds by almost an order of magnitude that of strain-free GaN and can be attributed to inhomogeneous microstrain originated by the coalescence of nuclei within the mask aperture [18]. Since the energy transitions change linearly with the strain component [19], the microstrain value should be of the order of $\pm 0.04\%$. Additionally, the PL broadening could arise from the random separation of the donor sites with respect to the lateral surfaces of the NWs [20]. The negligible variation of the FWHM with increasing d depicted in figure 3(b) suggests, nevertheless, that micro-strain is the most probable

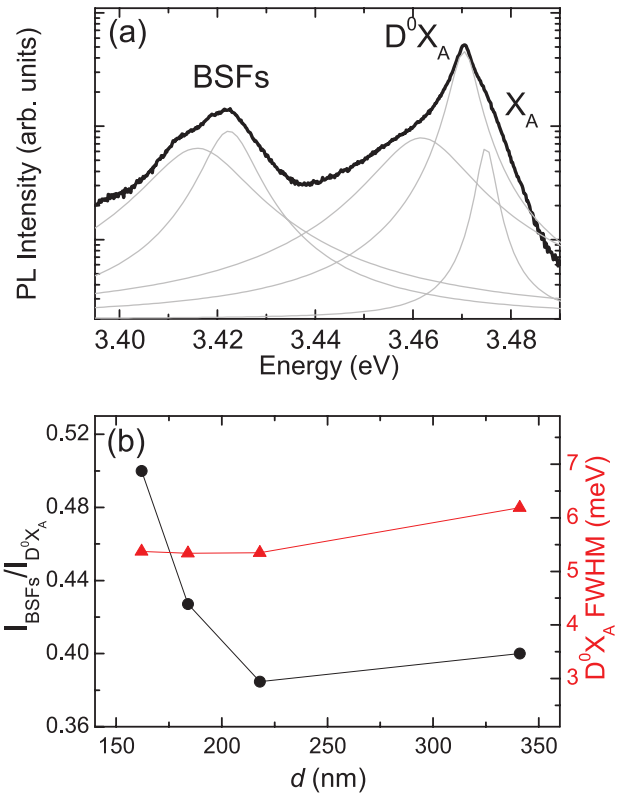

Figure 3. (a) Representative 5 K PL spectrum measured at low excitation power (2 μW) of NWs with $d = 220$ nm and $p = 0.15$ μm. (b) The integrated intensity of the emission from BSFs normalized to that from D^0X_A excitons and the FWHM of the D^0X_A emission as a function of d (fixed $p = 0.40$ μm).

cause of the FWHM of GaN SAG NW emission. The second band in figure 3(a) is a partially resolved doublet, composed of one peak at around 3.416 eV and the other at around 3.422 eV, attributed to BSFs. These extended defects are rare in *c*-plane GaN but appear with high density in nonpolar and semipolar samples [21–23]. BSFs can be seen as planar zinc-blende inclusions into the wurtzite GaN matrix which behave as type-II quantum wells ($\Delta E_C = 122$ meV, $\Delta E_V = -62$ meV, $L = 0.77$ nm) [23–25]. Thus the radiative recombination takes place between electrons confined in the stacking fault and holes localized in their vicinity.

The relative PL intensities of the described transitions recorded on different spots of the sample as a function of d and p show a consistent dependence on the mask geometry. The studies were limited to $p \leqslant 1$ μm, as for higher p self-organized NWs contributed significantly to the PL spectrum and invalidated any trend. Figure 3(b) shows how the ratio between the transitions involving BSFs and donor-bound excitons decreases with increasing d. However, the ratio is not affected by the mask p (not shown). This implies that variations in the local growth conditions derived from the arrangement of the apertures in the mask have a negligible impact on the density of BSFs. On the other hand, the dependence on the NW diameter points out the preponderance of the growth direction in the formation mechanism of BSFs. Thinner NWs, for which most of the growth takes place on semipolar facets, statistically present a higher BSF density. It is well reported that nonpolar structures contain a density of BSFs which can exceed that of polar structures by one to five orders of magnitude [26].

Finally, KPFM provides the contact potential difference between the metal tip and the material surface, i.e. the difference between their work functions. The work function of GaN changes with its crystal structure, polarity, doping level, presence of defects, and light exposure, among other parameters [27–29]. Figures 4(a) and (b) show the topography and its corresponding V_{CPD} maps of an extended array of SAG NWs. For most of the NWs, the six semipolar facets of the pyramidal tips are resolved in the topography image. The measured inclination of the tip facets with respect to the *c*-plane is of 42°, compatible with the wurtzite *r*-plane. A few of them show additional structure growing from the NW apex, as can be seen in figure 1(a). In order to avoid cross-talk artifacts with the topography, the vertical movement of the AFM tip was limited to 200 nm so that only the tips of the NWs could be imaged.

The V_{CPD} map of figure 4(b) correlates perfectly with the topography and GaN NWs are clearly distinguished from the Mo mask. An average positive V_{CPD} between 0.3–0.5 V is measured at the NW top surfaces, in good agreement with the Ga-polarity of these SAG NWs. The determination of GaN polarity from KPFM measurements is, nevertheless, a complex problem which will be analyzed in detail in a separate publication. The pyramid edges and apex are clearly resolved in figure 4(b) map since they present much lower V_{CPD} values, i.e., higher work functions. This gives an indication of the spatial resolution of these KPFM measurements (~40 nm). The higher density of dangling bonds at the joints of different facets could qualitatively explain the increase of the work function in these regions. Negative V_{CPD} are also obtained for the protuberant GaN material, identified as zinc-blende additional growth by TEM. In these cases the change in potential indicates different crystal structure. The higher level of noise recorded outside the NWs results from the larger distance between the AFM tip and the substrate, due to the limitation of its vertical movement.

A close-up analysis of the results reveals that a few of the otherwise apparently pristine NWs present subtle structure both in the topography and V_{CPD} of their pyramidal facets. Figures 4(c) and (d) show a comparative of two individual NWs, labeled 1 and 2, extracted from the topography map of figure 4(a). While NW 1 ends in perfectly smooth facets, NW 2 presents a sudden change in the facet inclination half way up in the NW tip. This change is better observed in the image of the AFM amplitude (figure 4(d) second image down) which acts as an error channel in our measurements. The semicircular shape of this structural defect is also reproduced in the V_{CPD} of NW2. Line profiles of the topography and V_{CPD} along the diameter of NW 2 are displayed in figure 4(e) showing that the facet inclination change coincides with a local minimum of V_{CPD}. The decrease in the V_{CPD} is qualitatively compatible with an increase in the work function produced by the lowering of the conduction band within the BSF. On the other hand, the measured facet angle with respect to the *c*-plane decreases from 42° to 35° coinciding with that of the wurtzite *r*-plane (43.2°) and a higher index zinc-blende plane, respectively.

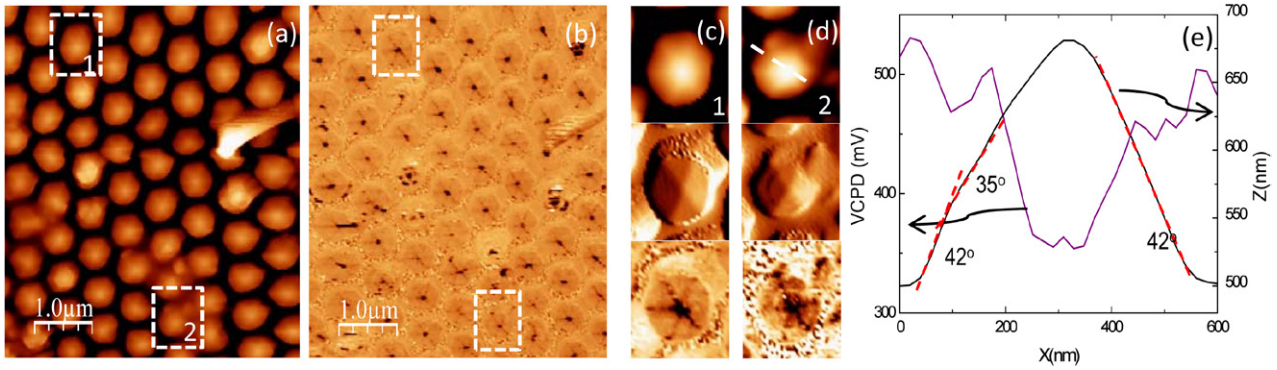

Figure 4. (a) Topography and (b) V_{CPD} of a $5 \times 5\ \mu m^2$ area with GaN SAG NWs with $d = 220$ nm and $p = 0.15\ \mu$m. The z-scale in each of the maps comprises 500–700 nm and 0–600 mV, respectively. A close-up of (from top to bottom) the topography, amplitude, and V_{CPD} of (c) NW1 and (d) NW2 are presented. (e) Profiles of the topography and V_{CPD} across NW 2 top surface following the line depicted in (d).

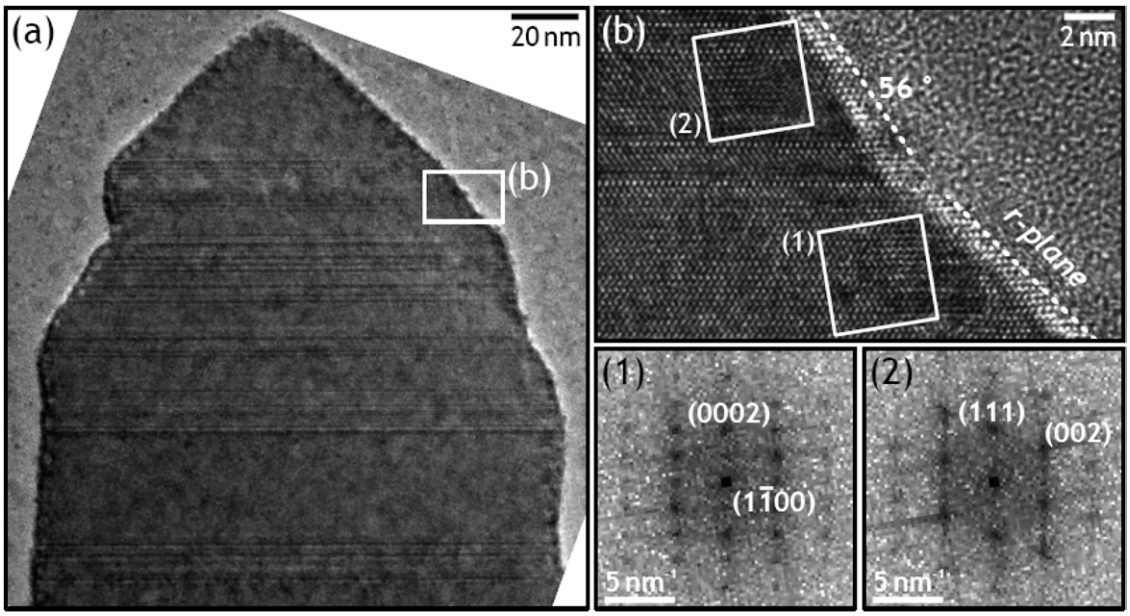

Figure 5. (a) High resolution TEM micrograph of the tip region of a NW with high density of defects. A higher magnification is shown in (b). Dashed lines indicate facet inclinations. Local fast Fourier transforms from the white boxed regions are shown below corresponding to hexagonal (1) and cubic (2) structures. The images have been rotated for clarity.

As shown in figure 5(a), BSFs can cause changes in the NW diameter in their vicinity and the shape of highly defective NWs can present an asymmetric shape or deviations from the *r*-plane facets. The fast Fourier transforms of figure 5(b) demonstrates that the change from hexagonal (1) to cubic (2) structure also induces a change in the facet angle. Therefore, the correlation between the angle mismatch and the deep observed in V_{CPD} in figure 4(e) constitutes a direct evidence of extended BSFs at the NW tip.

4. Conclusions

In summary, three different non-destructive probe techniques have been used for the structural characterization of GaN NWs grown by SAG MBE for different pitches and diameters of the mask apertures. The combination of these highly complementary techniques allows a detailed insight on the structural, optical and electronic properties of the global sample, as well as of individual NWs. The reduction of the mask pitch to values below twice the diffusion length of Ga atoms improved the growth selectivity but at the same time induced a slight deterioration of the crystal quality correlated with a reduction of the NW height. The reduction of the NW diameter, on the other hand, caused an increased weight of the emission from BSFs independently from the pitch. Since the completion of the pyramidal tip takes shorter times for thinner NWs, the presence of BSFs could be associated to the growth on semipolar planes. Finally, KPFM succeeded in locating and imaging extended defects, such as BSFs, at the semipolar top facets of individual NWs.

Acknowledgments

The research leading to these results has received funding from the European Union Seventh Framework Programme under “Nanowiring”, grant agreement number 265073.

References

[1] Li S and Waag A 2012 *J. Appl. Phys.* **111** 071101
[2] Bertness K A, Sanford N A and Davydov A V 2011 *IEEE J. Sel. Top. Quantum Electron.* **17** 847
[3] Calleja E, Sánchez-García M A, Sánchez F J, Calle F, Naranjo F, Muñoz E, Jahn U and Ploog K 2000 *Phys. Rev.* B **62** 24
[4] Brandt O, Pfüller C, Chéze C, Geelhaar L and Riechert H 2010 *Phys. Rev.* B **81** 045302
[5] Sekiguchi H, Kishino K and Kikuch A 2008 *Appl. Phys. Express* **1** 124002
[6] Kishino K, Sekiguchi H and Kikuchi A 2009 *J. Cryst. Growth* **311** 2063
[7] Schumann T, Gotschke T, Limbach F, Stoica T and Calarco R 2011 *Nanotechnology* **22** 095603
[8] Nagae Y, Iwatsuki T, Shirai Y, Osawa Y, Naritsuka S and Maruyama T 2011 *J. Cryst. Growth* **324** 88
[9] Bengoechea-Encabo A, Barbagini F, Fernández-Garrido S, Grandal J, Ristić J, Sánchez-García M A, Calleja E, Jahn U, Luna E and Trampert A 2011 *J. Cryst. Growth* **325** 89
[10] Hersee S D, Sun X and Wang X 2006 *Nano Lett.* **6** 1808
[11] Bengoechea-Encabo A, Albert S, Zuñiga-Perez J, de Mierry P, Trampert A, Barbagini F, Sánchez-García M A and Calleja E 2013 *Appl. Phys. Lett* **103** 241905
[12] Urban A, Malindretos J, Klein-Wiele J H, Simon P and Rizzi A 2013 *New J. Phys.* **15** 053045
[13] Colchero J, Gil A I and Baró A M 2001 *Phys. Rev.* B **64** 245403
[14] Placios-Lidón E, Abellán J, Munuera C, Ocal C and Colchero J 2005 *Appl. Phys. Lett.* **87** 154106
[15] Gotschke T, Schumann T, Limbach F, Stoica T and Calarco R 2011 *Appl. Phys. Lett.* **98** 103102
[16] Calleja J M *et al* 2007 *Phys. Status Solidi* **244** 2838
[17] Gogova D *et al* 2013 *J. Appl. Phys.* **113** 203513
[18] Jenichen B, Brandt O, Pfuller C, Dogan P, Knelangen M and Trampert A 2011 *Nanotechnology* **22** 295714
[19] Fernández-Garrido S, Kaganer V M, Hauswald C, Jenichen B, Ramsteiner M, Consonni V, Geelhaar L and Brandt O 2014 *Nanotechnology* **25** 455702
[20] Corfdir P, Lefebvre P, Ristić J, Valvin P, Calleja E, Trampert A, Ganiére J D and Deveaud-Plédran B 2009 *J. Appl. Phys.* **105** 013113
[21] Liu R, Bell A, Ponce F A, Chen C Q, Yang J W and Khan M A 2005 *Appl. Phys. Lett.* **86** 021908
[22] Paskov P P, Schifano R, Monemar B, Paskova T, Figge S and Hommel D 2005 *J. Appl. Phys.* **98** 093519
[23] Corfdir P, Lefebre P, Levrat J, Dussaigne D, Ganère J D, Martin D, Ristić J, Zhu T, Grandjean N and Deveaud-Plédran B 2009 *J. Appl. Phys.* **105** 043102
[24] Stampfl C and de Walle C G V 1998 *Phys. Rev.* B **57** R15052
[25] Salviati G *et al* 1999 *Phys. Status Solidi* **171** 325
[26] Polyakov A Y, Smirnov N B, Govorkov A V, Aamano H, Pearton S J, Lee I H, Sun Q, Han J and Karpov S Y 2011 *Appl. Phys. Lett.* **98** 072104
[27] Simpkins B S, Yu E T, Waltereit P and Speck J S 2003 *J. Appl. Phys.* **94** 1448
[28] Rodriguez B J, Yang W C, Nemanich R J and Gruverman A 2005 *Appl. Phys. Lett.* **86** 112115
[29] Wei J D, Li S F, Atamuratov A, Wehmann H H and Waag A 2010 *Appl. Phys. Lett.* **97** 172111